CHEMISTRY OF MATERIALS
Article

Chem. Mater. **2011,** *23,* 219–228 219
DOI:10.1021/cm102719k

Large Electric Field-Induced Strain and Antiferroelectric Behavior in $(1\text{-}x)(Na_{0.5}Bi_{0.5})TiO_3\text{-}xBaTiO_3$ Ceramics

Yiping Guo,[†,‡] Yun Liu,*[,†] Ray L. Withers,[†] Frank Brink,[§] and Hua Chen[§]

[†]*Research School of Chemistry, The Australian National University, Canberra, ACT 0200, Australia,* [‡]*State Key Laboratory of MMCs, Shanghai Jiaotong University, Shanghai 200240, China, and* [§]*Centre For Advanced Microscopy, The Australian National University, Canberra, ACT 0200, Australia*

Received September 21, 2010. Revised Manuscript Received November 29, 2010

The dielectric, ferroelectric, and electric field-induced strain response of $(1\text{-}x)(Na_{0.5}Bi_{0.5})TiO_3\text{-}xBaTiO_3$ (NBT-BT) ($0.04 \leq x \leq 0.10$) ceramics has been systematically investigated as a function of temperature. It is found that ferroelectric and antiferroelectric (AFE)-like behavior can coexist at temperatures significantly lower than the depolarization temperature T_d (even down to as low as ambient temperature). Electron microscopy suggests that such behavior results from the electric field-dependence of fine scale octahedral tilt twinning disorder and the associated disorder in the local (ferroic) off-center displacements of the Na/Bi/Ba and Ti ions. The existence of the AFE-like behavior significantly enhances the electric field-induced strain. High bipolar strain of 0.40% and unipolar strain of 0.27% has thereby been achieved at ambient temperature in an NBT-BT, $x = 0.07$, ceramic. The bipolar and unipolar strains reach almost identical maximum values when the temperature is close to T_d. Giant unipolar strains of 0.42%, 0.41%, and 0.29% were observed in NBT-BT ceramics with $x = 0.06$, 0.07, and 0.08 at temperatures close to their T_d's of 100 °C, 50 °C, and 87 °C, respectively. This work thus provides new insight into ways to further optimize lead-free NBT-BT piezoelectric ceramics for practical use in different temperature ranges.

1. Introduction

Lead-containing ceramics, in particular lead zirconate titanate ($PbZr_{1-x}Ti_xO_3$, PZT), are widely used in actuators, sensors, and transducers as a result of their excellent piezoelectric properties.[1,2] The serious effect on human health and the environment resulting from the toxicity of lead and lead oxides, however, is of ever increasing world-wide concern and makes it vital to develop replacement lead-free ceramics with comparable piezoelectric properties to those of PZT.

The $(1\text{-}x)(Na_{0.5}Bi_{0.5})TiO_3\text{-}xBaTiO_3$ (abbreviated as NBT-BT 100(1-x)/100x hereafter), $(1\text{-}x)(K,Na)NbO_3\text{-}xLi(Nb,Ta,Sb)O_3$ (KNN-LNTS), and small grain size $BaTiO_3$ systems are currently considered to be the most likely candidate systems for this purpose.[3−21] Of these candidate systems, the KNN-LNTS system at its morphotropic phase boundary (MPB) composition has the highest piezoelectric coefficient ($d_{33} \sim 240$ pC/N) and the highest electro-mechanical coupling coefficient ($k_p \sim 45\%$)[3−5] as well as good temperature stability of its piezoelectric properties.[13,14] KNN-based ceramics are thus currently the favored lead-free piezoelectric materials.

The processing required to reliably produce dense KNN-based ceramics, however, is quite challenging. By comparison, NBT-BT ceramics are much easier to densify. NBT-BT ceramics at its MPB composition, however, exhibit lower piezoelectric ($d_{33} \sim 160$ pC/N) and electro-mechanical coupling coefficients ($k_p \sim 36\%$), which diminish further above the relatively low depolarization temperature (T_d)

*E-mail address: yliu@rsc.anu.edu.au.

(1) Wanders, J. W. *Piezoelectric ceramics-properties and applications*; Philips Components: Eindhoven, 1991.
(2) Jaffe, B.; Cook, W. R.; Jaffe, H. *Piezoelectric Ceramics*; Academic: New York, 1971.
(3) Guo, Y.; Kakimoto, K.; Hitoshi, O. *Appl. Phys. Lett.* **2004**, *85*, 4121–4123.
(4) Guo, Y.; Kakimoto, K.; Hitoshi, O. *Mater. Lett.* **2005**, *59*, 241–244.
(5) Saito, Y.; Takao, H.; Tani, T.; Nonoyama, T.; Takatori, K.; Homma, T.; Nagaya, T.; Nakamura, M. *Nature* **2004**, *432*, 84–87.
(6) Xu, C.; Lin, D.; Kwok, K. W. *Solid State Sci.* **2008**, *10*, 934–940.
(7) Chen, M.; Xu, Q.; Kim, B. H.; Ahm, B. K.; Ko, J. H.; Kang, W. J.; Nam, O. J. *J. Eur. Ceram. Soc.* **2008**, *28*, 843–849.
(8) Chu, B. J.; Chen, D. R.; Li, G. R.; Yin, Q R. *J. Eur. Ceram. Soc.* **2002**, *22*, 2115–2121.
(9) Takenaka, T.; Maruyama, K.; Sakata, K. *Jpn. J. Appl. Phys.* **1991**, *30*, 2236–2239.
(10) Rödel, J.; Jo, W.; Seifert, T. P.; Anton, E.-M.; Granzow, T. *J. Am. Ceram. Soc.* **2009**, *92*, 1153–1177.
(11) Takahashi, H.; Numamoto, Y.; Tani, J.; Tsurekawa, S. *Jpn. J. Appl. Phys.* **2006**, *45*, 7405–7408.
(12) Karaki, T.; Yan, K.; Miyamoto, T.; Adachi, M. *Jpn. J. Appl. Phys.* **2007**, *46*, L97–L98.
(13) Zhang, S.; Xia, R.; Shrout, T. R.; Zang, G.; Wang, J. *Solid State Commun.* **2007**, *141*, 675–679.
(14) Higashide, K.; Kakimoto, K.; Ohsato, H. *J. Eur. Ceram. Soc.* **2007**, *27*, 4107–4110.
(15) Smolenskii, G. A.; Isupov, V. A.; Agronovskaya, A. I.; Krainik, N. N. *Soviet Phys.: Solid State* **1960**, *2*, 2982–2985.
(16) Vakhrushev, S. B.; Kvyatkovshii, B. E.; Okuneva, N. M.; Plachenova, E. L. *JETP Lett.* **1982**, *35*, 134–137.
(17) Emel'yanov, S. M.; Raevskii, I. P.; Smotrakov, V. G.; Savenko, F. I. *Soviet Phys.: Solid State* **1984**, *26*, 1151–1152.
(18) Isupov, V. A. *Ferroelectrics* **2005**, *315*, 123–147.
(19) Jones, G. O.; Thomas, P. A. *Acta Crystallogr., Sect. B: Struct. Sci.* **2002**, *58*, 168–178.
(20) Dorcet, V.; Trolliard, G. *Acta Mater.* **2008**, *56*, 1753–1761.
(21) Dorcet, V.; Troillard, G.; Boullay, P. *Chem. Mater.* **2008**, *20*, 5061–5073.

© 2010 American Chemical Society
Published on Web 12/22/2010

(~ 100 °C).[6−10] On the other hand, a very high, electric field induced strain response (~ 0.40%) has recently been reported in lightly KNN-doped, NBT-BT based ceramics by Zhang et al.[22−24] and also in pure NBT-BT based ceramics by Zhang et al.[25] The high magnitude of the electric field induced strain responses in these materials suggests a considerable potential for the practical usage of NBT-BT based ceramic materials as actuators. It is therefore of some considerable importance to systematically investigate and seek to understand this behavior.

Zhang et al.[22−24] attributed the observed high strain response in their lightly KNN-doped, NBT-BT based ceramics to a field induced, antiferroelectric (AFE) to ferroelectric (FE) phase transition caused by a disruption of the long-range FE order of NBT-BT upon addition of KNN. The same authors[25] also reported similar electric field-induced strain behavior in NBT-BT 94/6 ceramics but without the presence of KNN. The measured strain in this study was found to reach as high as 0.42% near the depolarization temperature T_d (100 °C), although it became quite low at ambient temperature (bipolar strain ~0.2% and unipolar strain ~0.1%). Recently, we have found that mixed FE and AFE-like behavior can be found even at ambient temperature in NBT-BT ceramics with $x = 0.07$ and 0.08. A giant bipolar strain up to 0.40% has thereby been obtained in NBT-BT 93/7 samples at ambient temperature. In this paper, we report these physical properties results and further systematically investigate the temperature dependence of the dielectric, ferroelectric, and strain behavior of NBT-BT ceramics.

On the structural side, in addition to physical properties studies, there has recently been careful temperature-dependent TEM studies of the various phase transitions in pure NBT ceramics by Dorcet et al.[20,21] These studies show that the reported low temperature rhombohedral ferroelectric to higher temperature tetragonal phase transition in NBT[19] is a two step phase transition process via an antiferroelectric-like, intermediate phase.[20,21] The transformation is reported to begin by a ".. reconstructive transformation of the rhombohedral phase into .. an intermediate modulated phase .. corresponding .. to rhombohedral perovskite blocks in which *Pnma* orthorhombic sheets are formed by a microtwinning process ..".[21] The formation of this intermediate modulated phase correlates with, and was thus proposed to be responsible for, the antiferroelectric and relaxor-like behavior of NBT observed over the 200−300 °C temperature range.[21] It is important to note that similar antiferroelectric and relaxor-like behavior has also been reported to occur in NBT-BT ceramics, but at significantly lower temperatures (~ 100 °C), close to its MPB composition.[6−8] Clearly the BT content of these NBT-BT ceramics strongly affects the temperature at which antiferroelectric-like behavior appears.[9] In this paper we therefore also report the results of a primarily electron diffraction study of these NBT-BT ceramics, particularly the samples close to the MPB region, in an attempt to understand the relationship between structure and function in these materials.

2. Experimental Section

Ceramics with nominal composition (1-x)NBT-xBT ($x = 0$, 0.04, 0.06, 0.07, 0.08, 0.10, and 0.12, abbreviated as NBT-BT 100(1-x)/100x hereafter) were synthesized by solid state reaction. High purity Na_2CO_3, Bi_2O_3, $BaCO_3$, and nano-TiO_2 (~ 20 nm) were used as starting materials. Mixtures of these starting materials in the appropriate ratio were first ball-milled for 5 h using ethanol as a medium followed by an initial calcination at 800 °C for 2 h. The calcined powder was then ball-milled again for 2 h and dried, followed by the addition of poly(vinylalcohol) as a binder. The resultant powder was then granulated and pressed into pellets with a diameter of 13 mm under a uniaxial pressure of 200 MPa. Finally, these pellets were sintered in air at 1150 °C for 2 h in a covered alumina crucible. The metric, or point group, symmetry of the resultant ceramic samples was investigated by X-ray powder diffraction (Siemens D-5000, Cu $K_{\alpha 1}$ radiation) using a scan step of 0.02° and a 2 h collection time for the 2θ range from 20° to 60°.

The resultant chemical compositions were confirmed via quantitative electron probe microanalysis (EPMA) in a scanning electron microscope (JEOL 6400) using $NaAlSi_3O_8$, Bi_2O_3, $BaSO_4$, and TiO_2 as compositional standards. For X-ray powder diffraction (XRD) measurement, as-sintered pelleted samples with a diameter of ~10 mm were polished and annealed in air at 500 °C for 4 h to eliminate strains caused by polishing. For investigation by electron microscopy, crushed powder samples were deposited onto holey-carbon coated Cu grids and examined using a Philips EM 430 TEM.

For electrical characterization, the pelleted samples were coated with silver paste on their surfaces and heat treated at 500 °C for 5 min to ensure good electrical contact. For piezoelectric measurements, the samples were immersed in silicone oil and poled by an electric field of 3.4 kV/cm. The electric field was applied over the temperature range 40−100 °C for 30 min. The piezoelectric constant d_{33} was measured using a Berlincourt-type quasi-static meter at approximately 55 Hz. The temperature dependence of the polarization-field (*P*-*E*) and strain-field (*S*-*E*) hysteresis loops as well as the associated switching current behavior was investigated on cooling from 150 °C. The measurement was carried out using an AixACCT ferroelectric test unit in conjunction with a laser interferometer. The sample was immersed in silicone oil to prevent arcing during the measurement. After unipolar strain characterization at 30 °C, the dielectric properties of the samples were measured using a high precision LCR meter (HP 4284A).

3. Results and Discussion

Figure 1 shows room temperature XRD patterns of the NBT-BT, $x = 0.0$, 0.04, 0.06, 0.07, 0.08, and 0.10, ceramic samples indexed with respect to the underlying parent perovskite substructure (labeled with the subscript p, p for parent perovskite substructure in what follows and taken using Cu $K_{\alpha 1}$ radiation, a scan step of 0.02° and a 2 h collection time for the 2θ range from 20° to 60°). With the resolution available to us, the patterns are in good agreement

(22) Zhang, S.; Kounga, A.; B.; Aulbach, E.; Ehrenberg, H.; Rödel, J. *Appl. Phys. Lett.* **2007**, *91*, 112906.
(23) Zhang, S.; Kounga, A. B.; Aulbach, E.; Granzow, T.; Jo, W.; Kleebe, H.-J.; Rödel, J. *J. Appl. Phys.* **2008**, *103*, 034107.
(24) Zhang, S.; Kounga, A. B.; Aulbach, E.; Granzow, T.; Jo, W.; Kleebe, H.-J.; Rödel, J. *J. Appl. Phys.* **2008**, *103*, 034108.
(25) Zhang, S.; Kounga, A. B.; Aulbach, E.; Deng, Y. *J. Am. Ceram. Soc.* **2008**, *91*, 3950–3959.

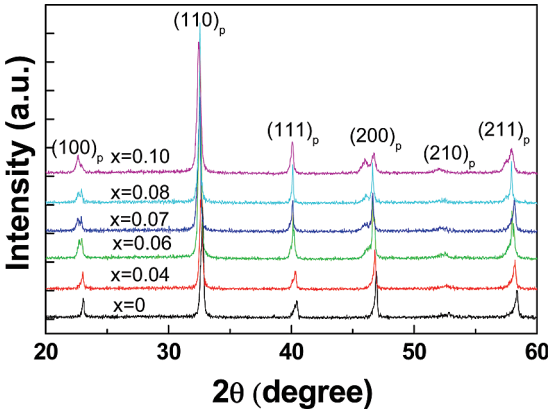

Figure 1. Room temperature XRD patterns of the NBT-BT, $x = 0.0$, 0.04, 0.06, 0.07, 0.08, and 0.10, ceramic samples indexed with respect to the underlying parent perovskite substructure (labeled with the subscript p, p for parent perovskite substructure in what follows).

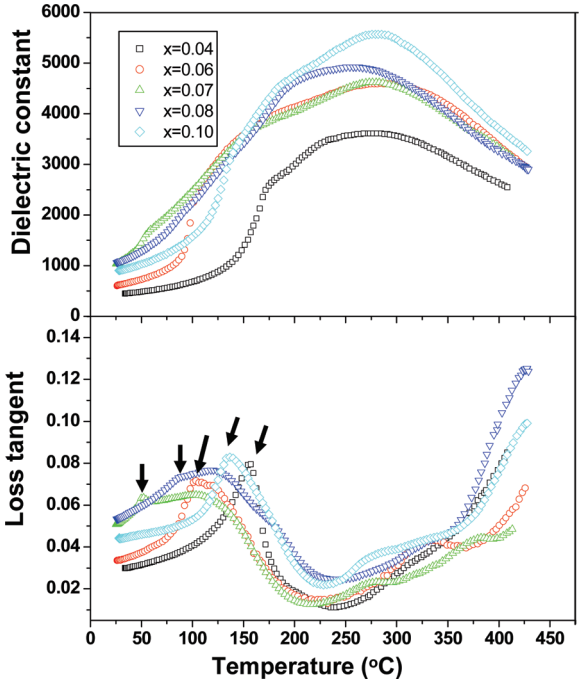

Figure 2. The dielectric constant and dielectric loss tangent curves (measured at 10 kHz) of poled NBT-BT, $x = 0.04$, 0.06, 0.07, 0.08, and 0.10, ceramic samples as a function of temperature. The arrows show the depolarization temperature (T_d) points.

with previously published XRD data (cf. Figure 1 with e.g. Figure 1 of refs 6 and 7). In particular, the clear asymmetric broadening to low angle of the $(111)_p$ peak (most apparent at low x and systematically diminishing with increasing x until it is only just apparent for the $x = 0.08$ and 0.10 samples) is consistent with splitting of this peak into the two peaks characteristic of the rhombohedral phase.[19] Likewise, the splitting of the asymmetrically broadened (at low x; see also e.g. Figure 1b of ref 7) but initially unsplit parent perovskite $(100)_p$ and $(200)_p$ peaks into two clearly split peaks, indicative of the significant presence of a tetragonal phase and the onset of the MPB region, is first apparent at the $x = 0.06$, NBT-BT 94/6 composition (*cf. e.g.* Figure 1 with Figure 1b of ref 7).

Table 1. Piezoelectric Constant d_{33}, Depolarization Temperature (T_d), Bipolar Strain (BS), and Unipolar Strain (US) of (1-x) NBT-x BT Ceramics[a]

x	0.04	0.06	0.07	0.08	0.10
d_{33} (pC/N)	95	139	180	148	138
T_d (°C)	155	100	50	87	135
BS (%)	0.07	0.25	0.40	0.28	0.28
US (%)	0.12	0.14	0.27	0.18	0.16

[a] T_d was determined from the temperature dependence of the loss tangent measured at 10 kHz (see Figure 1). The strain was measured at 30 °C under an electric field of 60 kV/cm and 1 Hz.

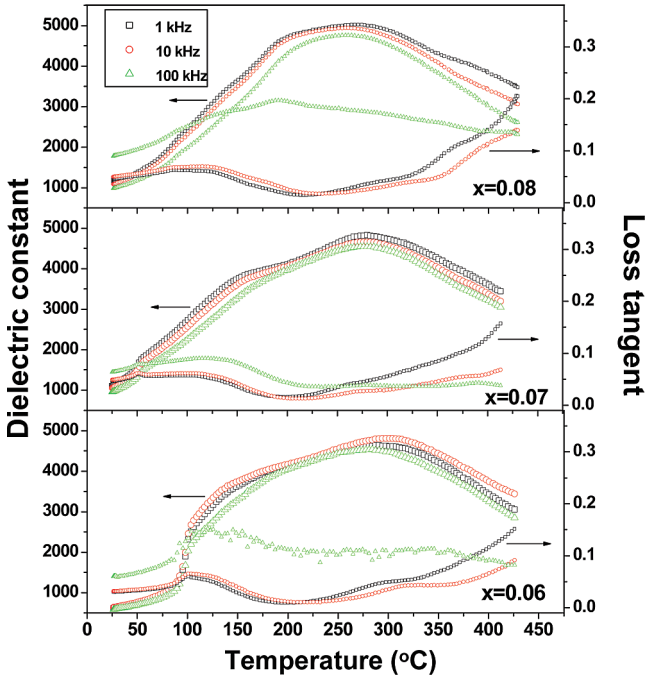

Figure 3. The temperature and frequency-dependent dielectric constant and dielectric loss tangent curves of poled NBT-BT (a) 94/6, (b) 93/7, and (c) 92/8 ceramic samples.

Thus there appears to be a slow, gradual transition from a predominantly rhombohedral ferroelectric phase into a predominantly tetragonal ferroelectric phase with increasing x or BT content. The low x ($x = 0$ and 0.04) samples appear to be predominantly in the rhombohedral ferroelectric phase, the highest x sample ($x = 0.10$) predominantly in the ferroelectric tetragonal phase while the samples closest to the MPB region ($x = 0.06$, 0.07, and 0.08) appear to exhibit a mixture of both rhombohedral and tetragonal phases. Such a conclusion is consistent with the electron diffraction evidence given below, in particular with the evidence for octahedral tilt twinning disorder.

Given the inherent, relatively fine scale structural disorder characteristic of these various 'phases' and the associated local stresses and strains, as revealed by the electron diffraction and imaging results shown later on, it is perhaps not surprising that metric symmetry is not entirely well-defined for NBT-BT samples.

Figure 2 shows the measured temperature dependence of the dielectric constant (ε_r) and dielectric loss tangent of the poled NBT-BT ($0.04 \leq x \leq 0.10$) samples measured at 10 kHz. Following Hiruma et al.,[26,27] the depolarization temperatures (T_d) of the various samples were defined as

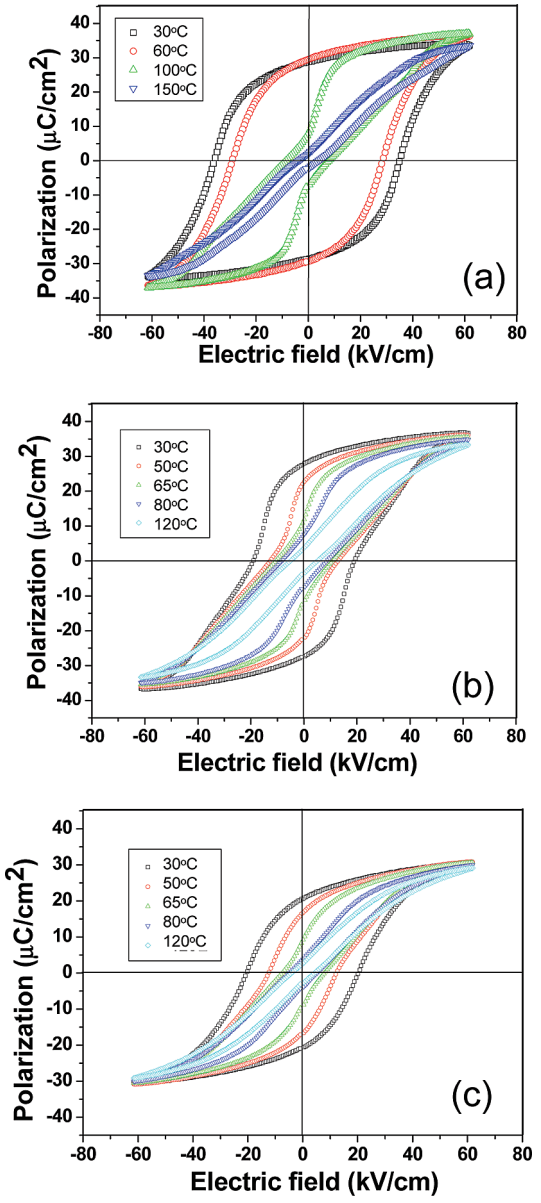

Figure 4. *P-E* polarization hysteresis loops as a function of temperature for the NBT-BT (a) 94/6, (b) 93/7, and (c) 92/8 ceramic samples. The frequency of the applied alternating current (AC) electrical field was 1 Hz.

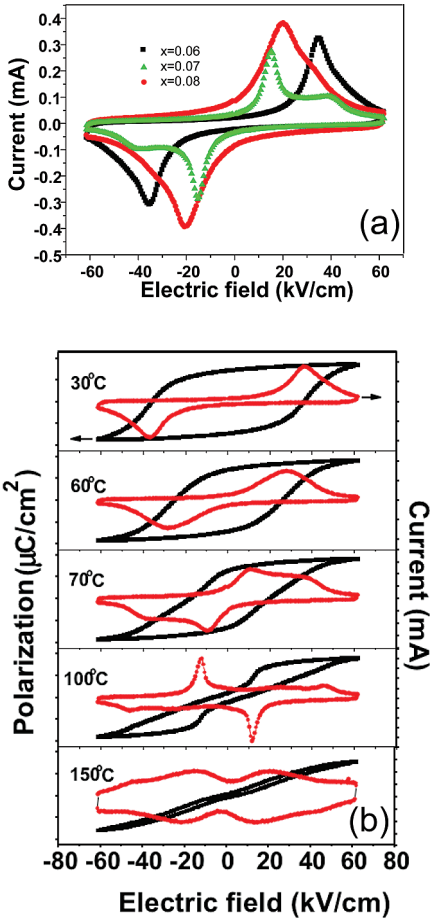

Figure 5. (a) The switching current (*I-V*) response of the NBT-BT 94/6, 93/7, and 92/8 ceramic samples measured under an electric field at a frequency of 1 Hz at 30 °C and (b) the switching current response of an NBT-BT 94/6 ceramic as a function of temperature, measured at 1 Hz during a cooling process.

the first inflection point (or peak) in the dielectric loss tangent curve of the poled samples as a function of increasing temperature. They are listed in Table 1 and labeled with arrows on the dielectric loss tangent curves in Figure 2. Note that these inflection points correspond to well-defined peaks in the dielectric loss tangent for the samples furthest away from the MPB region (the $x = 0.04$ and 0.10 samples). For the samples closest to the MPB region (the $x = 0.06$, 0.07, and 0.08 samples), however, these peaks in the dielectric loss tangent significantly broaden into plateau-like regions (mirrored also in the behavior of the dielectric constant) with the first inflection point defining the onset of the plateau-like region.

It is important to note that these first inflection points, and the corresponding T_d's, are not present in the corresponding unpoled samples, even for compositions close to the MPB region. Very similar behavior has recently been reported in closely related, doped NBT systems by Hiruma et al.[26,27] and suggests that depolarization in the vicinity of T_d arises from an electric field induced ferroelectric to intermediate antiferroelectric state.[6,28,29] Note that a low T_d may potentially enhance field-induced strain at room temperature while a strongly composition-dependent T_d in the vicinity of the MPB may have applications for designing actuators required to operate at different temperatures. Likewise it may be possible to adjust the peak in the dielectric constant (at T_m) via appropriate doping, although results to date (see e.g. Figure 2a) suggest that T_m is not as sensitive to doping.

Quantitative EPMA analyses of the synthesized NBT-BT samples showed that the concentrations of Na, Bi, Ba, and Ti were all within error of the nominal starting compositions, although there was some slight suggestion of a small deficiency in Na and corresponding smaller excess in Bi. The stoichiometry of the NBT-BT 93/7 sample, for example, was determined by EPMA to be

(26) Hiruma, Y.; Nagata, H.; Takenaka, T. *Jpn. J. Appl. Phys.* **2006**, *45*, 7409–7412.
(27) Hiruma, Y.; Nagata, H.; Takenaka, T. *J. Appl. Phys.* **2008**, *104*, 124106.
(28) Sakata, K.; Masuda, Y. *Ferroelectrics* **1974**, *7*, 347–349.
(29) Shrout, T. R.; Zhang, S. J. *J. Electroceram.* **2007**, *19*, 111–12.

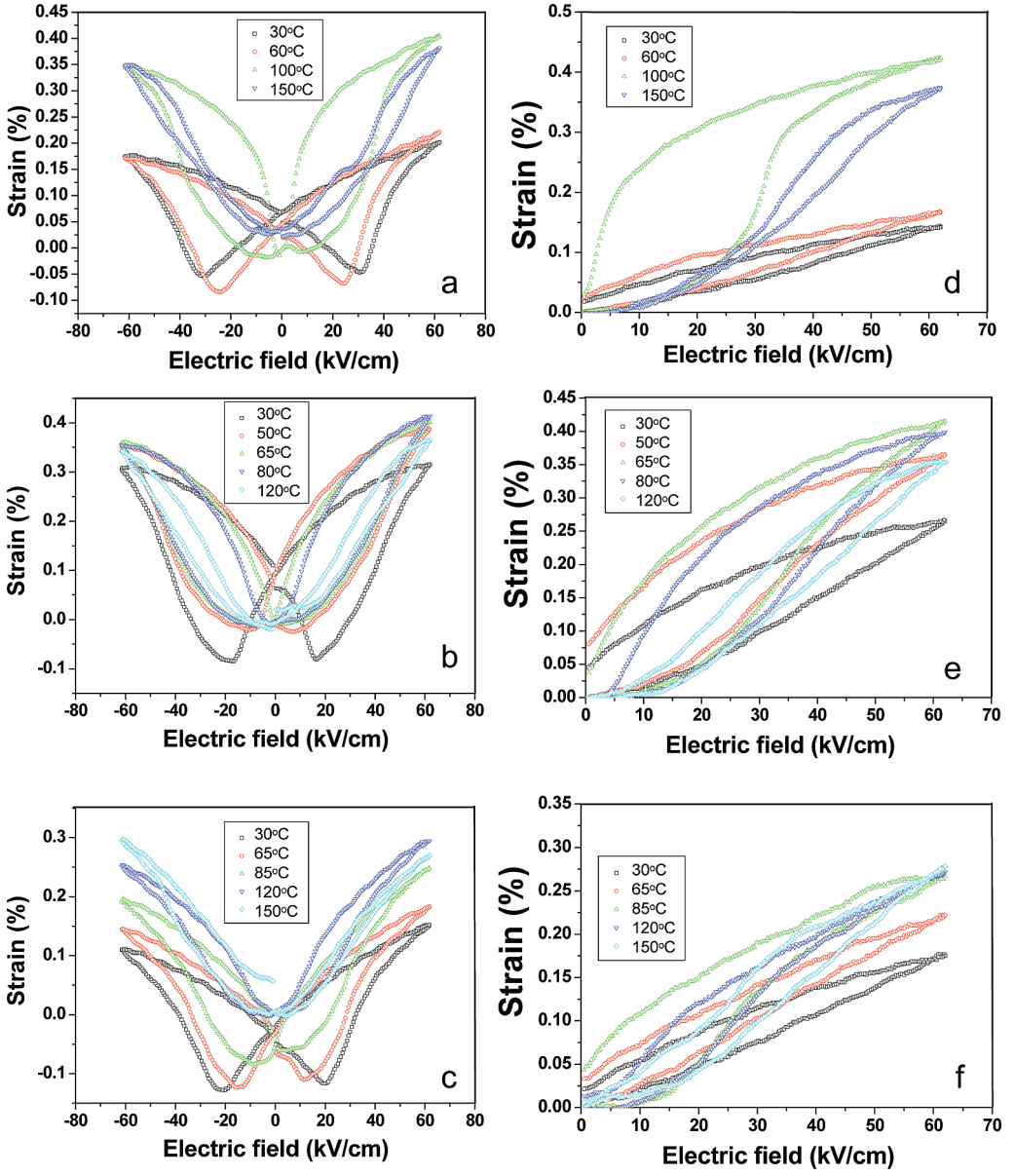

Figure 6. The bipolar (a-c) and unipolar (d-f) strain responses of the NBT-BT 94/6, 93/7, and 92/8 ceramic samples measured under an electric field at a frequency of 1 Hz and at different temperatures during cooling of the samples from 150 °C.

$Na_{0.44(3)}Bi_{0.48(2)}Ba_{0.07(1)}Ti_{0.99(2)}O_3$ compared to the nominal $Na_{0.465}Bi_{0.465}Ba_{0.07}TiO_3$ composition.

Figure 3 shows the temperature and frequency dependence of the dielectric constant and dielectric loss tangent of the poled NBT-BT (a) 94/6, (b) 93/7, and (c) 92/8 samples. Note the broadness, as well as the plateau-like shape, of the 'peak' in the dielectric constant as a function of temperature (at T_m) as well as the frequency-dependent behavior of the dielectric constant and dielectric loss tangent. This is strongly indicative of relaxor behavior. Note also the frequency-dependent behavior of both the dielectric constant and dielectric loss tangent. Figure 4 shows corresponding polarization-field (*P-E*) hysteresis loops for the NBT-BT (a) 94/6, (b) 93/7, and (c) 92/8 samples over a range of temperatures up to 150 °C. The corresponding switching current−voltage (*I-V*) curves were simultaneously collected as they are known to be more sensitive to polarization state. Typical *I-V* curves of different NBT-BT samples at ambient temperature as well as of the NBT-BT 94/6 sample measured at different temperatures are shown in Figure 5a and b respectively.

For the NBT-BT 93/7 sample, a pinched *P-E* hysteresis loop is apparent even at ambient temperature, 30 °C (see Figure 4b), suggesting the coexistence of FE and AFE-like, or even ferrielectric-like behavior.[30] This is clearly confirmed by the corresponding ambient temperature switching current curve shown in red in Figure 5a. For the NBT-BT 94/6 and 92/8 samples, the *P-E* loops at 30 °C appear saturated and to exhibit a typical *P-E* ferroelectric hysteresis loop character. The corresponding *I-V* curves (Figure 5a), however, suggest that some AFE-like character is also present in the NBT-BT 92/8 sample but not in the case of the NBT-BT 94/6 sample. These experimental results

(30) Onodera, A.; Cynshi, O.; Shiozaki, Y. *J. Phys. C* **1985**, *18*, 2831–2841.

thus strongly suggest the coexistence of both FE and AFE-like behavior in both the NBT-BT 93/7 and 92/8 samples at ambient temperature. The ambient temperature AFE-like character is most pronounced, however, at the NBT-BT 93/7 composition (as is apparent from Figure 5a).

On increasing temperature, this AFE-like character becomes ever more apparent in both the *P*-*E* hysteresis loops (see Figure 4) as well as the *I*-*V* curves (see Figure 5b) and at temperatures measurably lower than the depolarization temperatures, T_d, defined as the first inflection point (or peak) in the dielectric loss tangent curve of the poled samples and given in Table 1. In the case of the NBT-BT 94/6 sample, for example, the measured *I*-*V* curve shows clear AFE-like character at 70 °C, a temperature some 30 °C lower than its measured T_d as defined above (see Table 1). Thus AFE-like character can clearly appear at temperatures significantly lower than T_d in NBT-BT ceramics. Similar behavior has also been reported by Zhang et al. for their lightly KNN-doped, NBT-BT ceramics.[22−24]

The electric field-induced (a-c) bipolar and (d-f) unipolar strain-field (*S*-*E*) curves for the NBT-BT 94/6, 93/7, and 92/8 samples were also measured over a range of temperatures up to 150 °C, as shown in Figure 6. The bipolar *S*-*E* curves show the typical butterfly shape characteristic of FE materials at ambient temperature. On increasing temperature, however, this characteristic butterfly shape gradually changes. The "negative strain" i.e. the difference between the strain at zero field and the minimum value of the *S*(*E*) curve, gradually decreases as the temperature increases and eventually almost vanishes close to T_d. This suggests that the contribution of FE-like domain switching to the macroscopic strain becomes smaller with increasing temperature while the AFE-like domain switching contribution correspondingly becomes more significant, especially when the temperature is close to T_d. This enhanced strain effect is clearly associated with the onset of AFE-like behavior in the vicinity of T_d.

This is in good agreement with the frequency-dependent dispersive behavior of the dielectric-temperature spectra shown in Figure 3, where the dielectric dispersion behavior becomes noticeably weaker below T_d. This behavior differs from that of the unpoled samples where the dielectric dispersion behavior shows no significant change on cooling, as reported previously.[31] Such behavior implies the appearance of electric field induced, long-range ordered, polarization states induced by poling. NBT-BT samples with compositions closest to the MPB appear to have FE and AFE states coexisting even at room temperature. On poling, the AFE state appears to partially convert into a metastable FE state at room temperature. A phase transition from this metastable FE state into the AFE state then occurs at T_d, leading to the anomaly observed in the dielectric spectra as a function of temperature.

Figure 7 shows the measured maximum values of the bipolar and unipolar strains (S_{max}) of the NBT-BT,

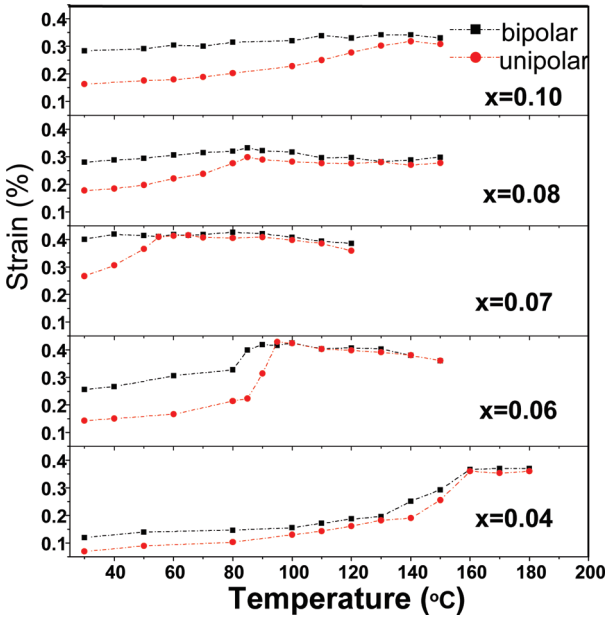

Figure 7. The temperature dependence of the maximum strains (S_{max}) of the NBT-BT, x = 0.04, 0.06, 0.07, 0.08, and 0.10, ceramic samples.

x = 0.04, 0.06, 0.07, 0.08, and 0.10, ceramic samples as a function of temperature. Note that the measured bipolar strains are significantly higher than the values of the unipolar strain at ambient temperature (see also Table 1). Note also that both the bipolar (see Figure 6a-c and Figure 7) as well as the unipolar strains (see Figure 6d-f and Figure 7) increase with increasing temperature, reaching a maximum value in the vicinity of the depolarization temperature, T_d, and then gradually decreasing with any further increase in temperature.

Figure 8 shows (a) $\langle -130 \rangle_p$ and (b) $\langle 111 \rangle_p$ zone axis electron diffraction patterns (EDP's) typical of the rhombohedral ferroelectric NBT (x = 0) end-member phase (*cf. e.g.* with Figures 4 and 5 of Dorcet et al.;[21] note that the indexation in Figure 8 is with respect to the underlying parent perovskite substructure). (c) and (d) show the equivalent EDP's typical of the metrically tetragonal, 93/7 (x = 0.07) sample, the sample which exhibits both FE and AFE-like behavior at ambient temperature (see e.g. Figure 5).

Note the presence of strong $\mathbf{G} \pm {}^1/_2[111]_p^*$ type satellite reflections (arrowed in Figure 8a) associated with $a^-a^-a^-$ octahedral tilting (i.e., octahedral tilting around a parent perovskite $\langle 111 \rangle_p$ direction, see e.g. ref 21) along with characteristic diffuse streaking (running along the $\langle 001 \rangle_p^*$ directions of reciprocal space) linking these satellite reflections with rather broader and much weaker $\mathbf{G} \pm {}^1/_2 \langle 110 \rangle_p^*$ 'satellite reflections' (note: **G** here represents the set of parent perovskite Bragg reflections). Note that these very weak $\mathbf{G} \pm {}^1/_2 \langle 110 \rangle_p^*$ type 'satellite reflections' are only just visible in the $\langle 111 \rangle_p$ zone axis EDP shown in Figure 8b.

In the case of the 93/7 (x = 0.07) sample, the situation is reversed, and the $\mathbf{G} \pm {}^1/_2 \langle 111 \rangle_p^*$ 'satellite reflections' are now much weaker and appear to be slightly extended perpendicular to the $\langle 001 \rangle_p^*$ direction of reciprocal space, whereas the previously weak $\mathbf{G} \pm {}^1/_2 \langle 110 \rangle_p^*$ type 'satellite

(31) Hiruma, Y.; Watanabe, Y.; Nagata, H.; Takenaka, T. *Key Eng. Mater.* **2007**, *350*, 93–96.

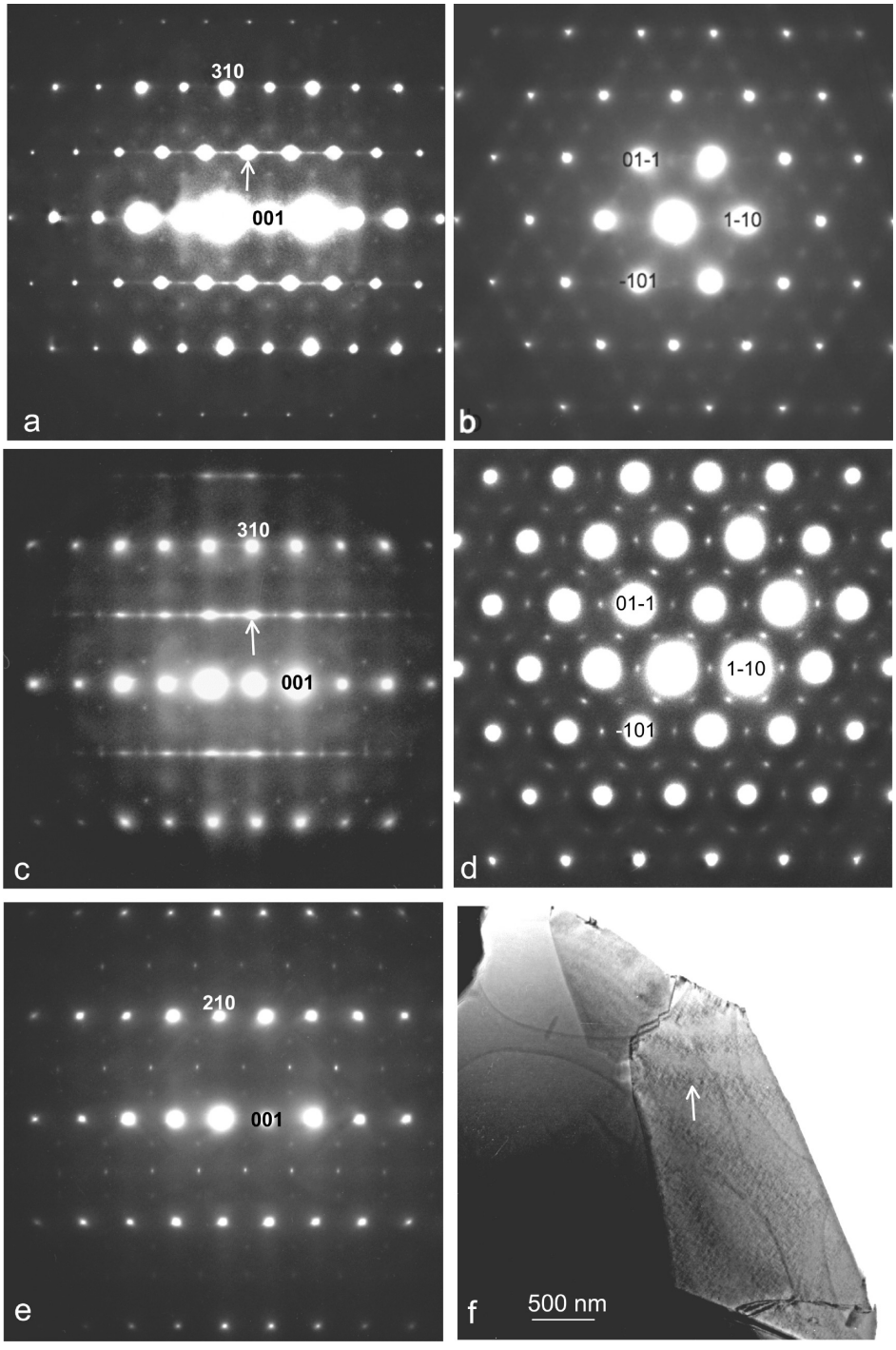

Figure 8. (a) $\langle -130 \rangle_p$ and (b) $\langle 111 \rangle_p$ zone axis EDP's of the rhombohedral ferroelectric NBT ($x = 0$) end-member phase. Equivalent (c) $\langle -130 \rangle_p$ and (d) $\langle 111 \rangle_p$ zone axis EDP's of the 93/7 ($x = 0.07$) sample. (e) shows a $\langle -120 \rangle_p$ zone axis EDP and (f) a Bright Field (BF) image typical of the 93/7 ($x = 0.07$) sample. Indexation in Figure 8 is with respect to the underlying parent perovskite substructure.

reflections' (arrowed in Figure 8c), and associated with octahedral tilting around the $\langle 001 \rangle_p$ direction, are now strong although quite significantly broadened along the $\langle 001 \rangle_p^*$ direction. The essentially continuous diffuse streaking linking the $\mathbf{G} \pm {}^1/_2 \langle 111 \rangle_p^*$ and $\mathbf{G} \pm {}^1/_2 \langle 110 \rangle_p^*$ 'satellite reflections', however, is still present and implies the presence of considerable octahedral tilt twinning disorder along the corresponding $\langle 001 \rangle$ real space direction. Note that the $\mathbf{G} \pm {}^1/_2 \langle 110 \rangle_p^*$ 'satellite reflections' are now clearly visible in the $\langle 111 \rangle_p$ zone axis EDP shown in Figure 8d (*cf.* with Figure 8b) and broadened perpendicular to the relevant $\langle 110 \rangle^*$ directions of reciprocal space.

It is important to note that fine scale octahedral tilt twinning disorder, as implied by the existence of the very broad $\mathbf{G} \pm {}^1/_2 \langle 110 \rangle_p^*$ 'satellite reflections', will locally create a distinctly different environment for the Na/Bi/Ba ions at the {001} twin boundaries and hence for the local off-center cation displacements giving rise to local ferroic behavior. The electric field dependence of this octahedral tilt twinning disorder and the associated disorder in the local displacements of the Na/Bi/Ba and Ti ions is thus

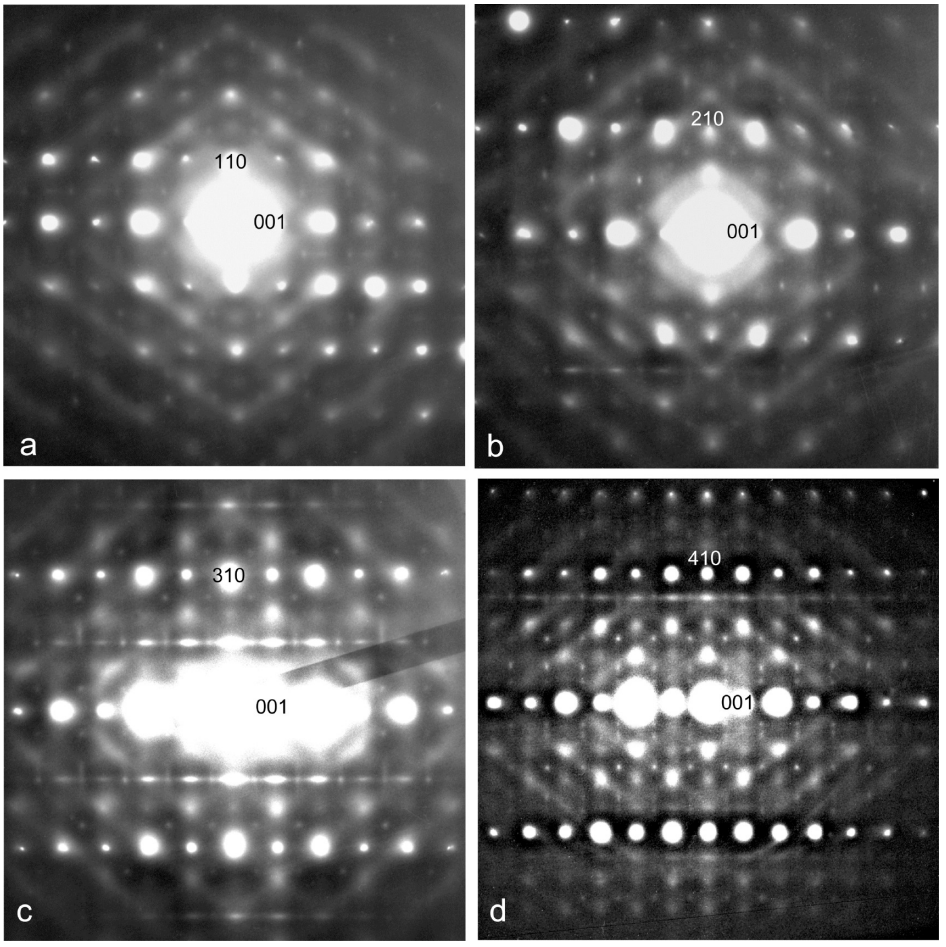

Figure 9. (a) Close to ⟨−110⟩, (b) ⟨−120⟩, (c) ⟨−130⟩, and (d) ⟨−140⟩ zone axis EDP's typical of the tetragonal 90/10 ($x = 0.1$) sample. Indexation in Figure 9 is again with respect to the underlying parent perovskite substructure.

most probably the cause of the observed coexisting FE and AFE-like (or ferrielectric[30]) behavior observed in the ambient temperature *P-E* hysteresis loops and switching current behavior of this sample.

Figure 8e shows a $\langle -120 \rangle_p$ zone axis EDP and Figure 8f a Bright Field (BF) image typical of the 93/7 ($x = 0.07$) sample. Note that the $\mathbf{G} \pm {}^1/_2 \langle 011 \rangle_p^*$ type 'satellite reflections' are again present in Figure 8e and the existence of weak diffuse streaking/banding running through the parent perovskite Bragg reflections perpendicular to ⟨001⟩*. The same weak diffuse streaking/banding is also apparent in Figure 8c although not in Figure 8a. The presence of such weak $\mathbf{G} \pm \{001\}^*$ diffuse intensity may be due to 1-D correlated off-center displacements of the perovskite *A* (Bi/Na/Ba) and *B* (Ti) ions along the ⟨001⟩ directions. Finally, note also the large scale tetragonal microdomains in Figure 8f along with the presence of a much finer scale tweed-like microstructure inside the individual tetragonal domains (arrowed in Figure 8f).

It is important to note that there is no evidence for separate ferroelectric and antiferroelectric phases coexisting within this 93/7 ($x = 0.07$) sample at ambient temperature. The apparent FE and AFE-like behavior in e.g. the ambient temperature switching-current behavior of this sample must therefore somehow be associated with electric field-induced changes in the octahedral tilt twin disorder and the effect this has upon the local off-center dispacements of the Na/Bi and Ti ions responsible for ferroelectric and antiferroelectric-like behavior in the measured physical properties.

Figure 9 shows (a) close to ⟨−110⟩, (b) ⟨−120⟩, (c) ⟨−130⟩, and (d) ⟨−140⟩ zone axis EDP's typical of the tetragonal 90/10 ($x = 0.1$) sample. The ⟨−120⟩ and ⟨−130⟩ EDP's shown in Figure 9b and c appear rather similar to the equivalent $x = 0.07$ zone axis EDP's shown in Figure 8e and c except for the existence of a highly structured, transverse polarized, diffuse intensity distribution taking the form of $\mathbf{G} \pm \{111\}^*$ sheets of diffuse intensity. Cuts through these $\mathbf{G} \pm \{111\}^*$ sheets of diffuse intensity give rise to the clearly visible diffuse streaking running along the ⟨112⟩*, ⟨213⟩*, ⟨314⟩*, and ⟨415⟩* directions of reciprocal space in Figure 9a,b,c, and d, respectively. Note that this diffuse streaking runs largely only through the $h+k+l$ even, but not odd, parent Bragg reflections.

Such a diffuse distribution is strongly reminiscent of a very similar diffuse distribution characteristic of PZT itself as well as La-doped PZT i.e. PLZT.[31,32] The structural origin of this diffuse distribution is shown in these

(32) Welberry, T. R.; Goossens, D. J.; Withers, R. L.; Baba-Kishi, K. Z. *Metal. Mater. Trans.* **2010**, *41*, 1110–1118.

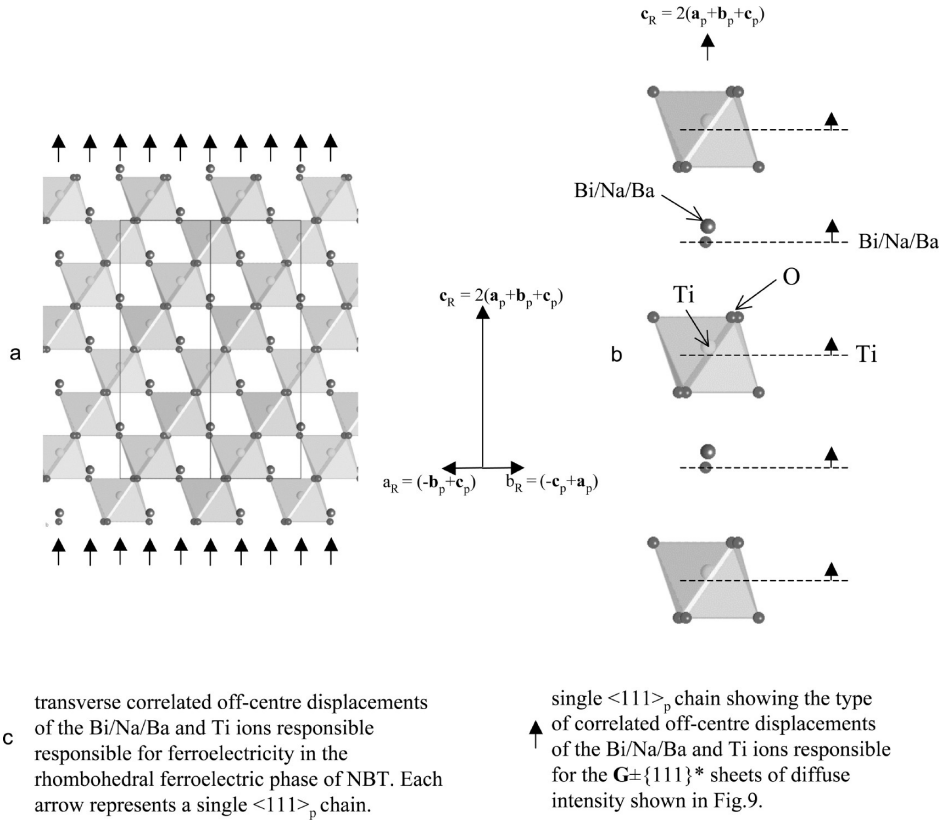

Figure 10. The right-hand side (b) shows the 1-D correlated off-center displacements of the Bi/Na/Ba and Ti ions along the $\langle 111 \rangle_p$ directions responsible for the characteristic $\mathbf{G} \pm \{001\}$* diffuse distribution apparent in the EDP's shown in Figure 9. The left-hand side (a) shows the rhombohedral ferroelectric pattern of off-center cation displacements that result if the 1-D chains are transverse correlated from one chain to the next. (c) is a schema showing the relationship between the 1-d chains and the transverse correlated ferrolectric phase.

papers to be due to 1-D correlated off-center displacements of the perovskite *A* (Bi/Na/Ba) and *B* (Ti) ions along the ⟨111⟩ directions (as shown in Figure 10). The observed diffuse distribution requires that the off-center displacements of the Bi/Na/Ba and Ti ions must be correlated along the 1-D chains (one of which is shown on the right-hand side of Figure 10) but not correlated at all from one such chain to the next. Intriguingly, if such chains were correlated from one chain to the next (as shown on the left-hand side of Figure 10), the $\mathbf{q} = \mathbf{0}$ mode responsible for ferroelectricity in rhombohedral NBT-BT would result (see the left-hand side of Figure 10). This suggests that long-range rhombohedral ferroelectric order of rhombohedral type has been destroyed by $x = 0.10$, although short-range remnants in the form of 1-D polar nanoregions (PNR's) obviously remain even on the tetragonal side of the MPB region. It is possible that these PNR's may be associated with the relaxor behavior apparent in Figure 3.

It is important to note that the above results are internally self-consistent. First, the gradual distortion of the *P-E* hysteresis loops cannot be attributed to the existence of extrinsic or point defects. If that were true, the first inflection points in the dielectric loss tangent curves should not be observed. Second, without the existence of an antiferroelectric-like contribution, it would not be possible to either observe, or explain, why the negative strain should systematically become smaller and finally decrease to zero as a function of increasing temperature. The observed behavior requires that FE and AFE-like polarization states can coexist at temperatures significantly lower than T_d. This conclusion is in good agreement with ref 33 where the dielectric-temperature spectra of unpoled NBT-BT samples measured under a "weak electric field" also show a T_d transition. They also assign this transition to a gradual ferroelectric to antiferroelectric transformation on increasing temperature with the transition being mostly complete near T_d.

The highest ambient temperature bipolar strain of 0.40% and unipolar strain of 0.27% obtained in this study was from the NBT-BT 93/7 sample at 30 °C, implying the existence of AFE-like behavior is extremely important for the observed strain behavior. The measured bipolar and unipolar strains of the NBT-BT 93/7 samples continue to increase with increasing temperature, reaching maximum values near T_d of 0.42% and 0.41%, respectively. Furthermore, giant unipolar strains of 0.42% and 0.29% were also observed in the NBT-BT 94/6 and 92/8 samples, respectively, once the temperature becomes close to the corresponding T_d.

The results reported in this paper show that (1-*x*)NBT-*x*BT ceramics with a very high strain response can be

(33) Withers, R. L.; Liu, Y.; Welberry, T. R. *J. Solid State Chem.* **2009**, *182*, 356–363.
(34) Ma, C.; Tan, X. *Solid State Commun.* **2010**, *150*, 1497–1500.

achieved at ambient as well as at higher temperatures and that the temperature at which the maximum strain response occurs can be systematically adjusted by adding different amounts of BT. The results therefore suggest that (1-x)-NBT-xBT lead free piezoelectric ceramics have considerable potential for use over a range of different temperatures.

Finally, we note that the highest, ambient temperature d_{33} value was also achieved in the NBT-BT sample with the lowest T_d value (see Table 1), i.e. the 93/7 sample, suggesting that high d_{33} values can also be attributed to the close proximity of the phase boundary between FE and AFE states. In the case of NBT itself, this 'phase boundary' has been shown by Dorcet et al.[20,21] to be due to " .. a phase transition involving the reconstructive transformation of the rhombohedral (ferroelectric) phase into an intermediate modulated phase .. corresponding to an intergrowth of rhombohedral blocks in which orthorhombic sheets are formed by a microtwinning process ..".[21] Further higher resolution, temperature-dependent, TEM and other investigations are under way in a bid to further understand the mechanism underlying the apparent coexistence of FE and AFE-like behavior in the NBT-BT, $x \sim 0.07$, system at ambient temperature.

4. Conclusions

The dielectric, ferroelectric, and electric field-induced strain behavior of NBT-BT ceramics ($0.04 \leq x \leq 0.10$) have been systematically investigated over a broad temperature range. It is found that FE and AFE-like behavior can coexist at temperatures significantly lower than the apparent depolarization temperature T_d, even down to as low as ambient temperature, and that the coexistence of FE and AFE-like behavior clearly enhances electric field-induced strain response. Electron microscopy shows no evidence for separate FE and AFE states but rather suggests that the observed behavior results from the electric-field dependence of the octahedral tilt twinning disorder and associated disorder in the local displacements of the Na/Bi/Ba and Ti ions. The highest ambient temperature bipolar strain of 0.40% and unipolar strain of 0.27% were achieved in NBT-BT samples with $x = 0.07$. The FE-like behavior gradually transformed into AFE-like behavior with increase in temperature until the transition was largely complete at T_d. As a result, the measured bipolar and unipolar strains reach almost identical maximum values when the temperature is close to the depolarization temperature of the relevant NBT-BT ceramic. Giant unipolar strains of 0.42%, 0.41%, and 0.29% were observed in $x = 0.06$, 0.07, and 0.08 NBT-BT ceramics in the vicinity of their respective depolarization temperatures of 100 °C, 50, and 87 °C.

The electric field-induced strain in (1-x)NBT-xBT ceramics at particular temperatures can therefore be controlled by adding different amounts of BT to adjust the relative amounts of the FE and AFE-like polarization states. This work thus offers an opportunity for lead free NBT-BT piezoelectric ceramics to be optimized for practical use in actuators operating at different temperatures.

Acknowledgment. Y.P.G., Y.L., and R.L.W. thank the Australian Research Council (ARC) for financial support in the form of ARC Discovery Grants. Y.P.G. also appreciates support from the Pujiang scholar foundation of Shanghai (No. 08PJ1407100).